Forcing and feedback in the MPI-ESM-LR coupled model under abruptly quadrupled CO_2

K. Block[1,2] and T. Mauritsen[1]

Received 1 August 2012; revised 21 June 2013; accepted 1 July 2013.

[1] Radiative feedback mechanisms associated with temperature, water vapor, cloud, and surface albedo change determine climate sensitivity to radiative forcing. Here we use the linearized radiative kernel-technique in combination with a Gregory analysis to determine the strength and structure of feedbacks, as well as direct and adjusted CO_2 forcings in the coupled Max Planck Institute Earth System Model at base resolution (MPI-ESM-LR). We show that the combined Kernel-Gregory approach yields an elegant separation of surface temperature-dependent feedbacks from contributions to radiative forcing by fast adjustments. MPI-ESM-LR exhibits a relatively large cloud adjustment of nearly 2 W m^{-2} in direct response to quadrupled CO_2, with positive cloud adjustment evident throughout the tropics, subtropics and over most landmasses whereas midlatitude storm tracks contribute negatively. The model features a nonlinear regression of radiation imbalance to global mean surface temperature change, resulting in a significantly increasing effective climate sensitivity after about 20 years which is approximately at temperatures 4–5 K above preindustrial. This feature is not uncommon among climate models and is relevant for future climate projections. We analyze the contribution of the individual feedback processes to this behavior and discuss possible origins such as differential ocean warming patterns associated with deep-ocean heat uptake or state dependencies of the feedback processes.

Citation: Block, K., and T. Mauritsen (2013), Forcing and feedback in the MPI-ESM-LR coupled model under abruptly quadrupled CO_2, *J. Adv. Model. Earth Syst.*, *5*, doi:10.1002/jame.20041.

1. Introduction

[2] Climate sensitivity, defined as the equilibrium temperature response to the radiative forcing from a doubling of atmospheric CO_2 concentration, is determined by a set of feedback mechanisms. As temperatures rise, the climate system emits more longwave radiation to space (temperature feedback), thereby reducing the initial radiation imbalance. A warmer atmosphere may contain more water vapor, which itself is a greenhouse gas (water vapor feedback), and causes snow and sea ice to retreat leading to more absorption of sunlight (surface albedo feedback). Both the water vapor and surface albedo feedback act to amplify warming. In addition, shifts in the cloud fields can act to either amplify or dampen climate change by regulating the flows of energy into and out of the climate system (cloud feedback). Spread in climate sensitivity between global climate models has been shown to be due mainly to intermodel variations in cloud feedback [e.g., *Cess et al.*, 1990; *Colman*, 2003; *Soden and Held*, 2006; *Dufresne and Bony*, 2008; *Soden et al.*, 2008].

[3] It is useful to think of the climate system as a box model describing the Earth's radiation imbalance (ΔR) at the top of the atmosphere (TOA) in relation to the global mean surface temperature change (ΔT_s) after an external radiative forcing (F) has been applied:

$$\Delta R = F + \lambda \Delta T_s, \tag{1}$$

where λ is the total feedback factor, which must be negative to yield a stable climate. *Gregory et al.* [2004] suggested that forcing and feedback can be analyzed from the transient behavior of the climate system in experiments where a forcing is abruptly applied to a system that is initially at steady state. F and λ can then be directly inferred by regressing ΔR on ΔT_s as the system relaxes toward a new steady state. This approach differs from studies that compare near-equilibrium states before and after a radiative forcing has been applied [e.g., *Colman*, 2003; *Soden and Held*, 2006; *Soden et al.*, 2008].

[4] Classical analysis [e.g., *Hansen et al.*, 1997; *Stuber et al.*, 2001; *Forster et al.*, 2007] would assume that

[1]Max Planck Institute for Meteorology, Hamburg, Germany.
[2]Institute for Meteorology, Universit ät Leipzig, Leipzig, Germany.

1942-2466/13/10.1002/jame.20041

forcing from CO_2 is due only to the direct radiative forcing and fast stratospheric temperature adjustment, which is nearly model independent. However, a key finding in applications of the Gregory method is that adjusted CO_2 forcing varies considerably among climate models due to fast cloud adjustment [*Gregory and Webb*, 2008]. Therefore, part of the cloud-induced radiation imbalance is to be considered a contribution to forcing, while another part is a surface temperature-dependent feedback [*Colman and McAvaney,* 2011].

[5] After abruptly applying a forcing many coupled atmosphere-ocean climate models exhibit a nonlinear evolution with a steeper slope in the first decades and a more shallow slope subsequently [*Andrews et al.*, 2012]. This behavior has previously been attributed to decadal ocean adjustments associated with transient differential patterns of warming, for instance induced by regional deep ocean heat uptake [*Senior and Mitchell*, 2000; *Williams et al.,* 2008], suggesting that the forcing (F) changes in time [*Winton et al.,* 2010]. This suggestion makes an interpretation within the simple conceptual framework (Equation (1)) challenging. It is, however, also possible that the processes determining the total feedback factor (λ) are functions of state or radiation imbalance. Sea ice for instance is initially bounded by the continents [*Eisenman et al.,* 2011] and may eventually disappear altogether, thereby inducing a nonlinear feedback. Also, cloud and water vapor feedbacks could potentially strengthen in warmer climates [*Abbot et al.,* 2009; *Jonko et al.,* 2013]. Furthermore, some models do indicate increasing forcing from a doubling of CO_2 in warmer climates [*Hansen et al.,* 2005; *Colman and McAvaney,* 2009]. The abundance of possible influencing factors motivates further studies.

[6] The objectives of the present study are to document climate change feedback factors as well as contributions to total CO_2 forcing from fast adjustments in the coupled Max Planck Institute Earth System Model (MPI-ESM-LR) [*Giorgetta et al.,*, 2013]. Further, the nonlinear behavior during the course of a simulation with abruptly quadrupled CO_2 is investigated. For these purposes, a combination of the radiative kernel technique [*Shell et al.,* 2008; *Soden et al.,* 2008] and the Gregory analysis [*Gregory et al.*, 2004] permits us to separate fast adjustments from the individual surface temperature-dependent feedback mechanisms as the climate evolves toward a new steady state. In many ways, this technique is similar to that of *Colman and McAvaney* [2011], who used the partial radiation perturbation technique instead of kernels, in another model that did not exhibit increasing climate sensitivity.

2. Methods

[7] A computationally efficient method to diagnose radiative feedbacks is to evaluate partial derivatives of TOA radiation with respect to atmospheric temperature, surface temperature, water vapor, surface albedo, and CO_2. These radiative kernels are multiplied with the respective changes in the state variables to quantify the various feedbacks [e.g., *Held and Soden*, 2000; *Soden and Held*, 2006; *Shell et al.*, 2008; *Soden et al.*, 2008].

2.1. Deriving and Applying Radiative Kernels

[8] The technique of computing radiative kernels is implemented into the radiative transfer scheme of the atmospheric component of MPI-ESM-LR - the atmospheric general circulation model ECHAM6 [*Stevens et al.,* 2013], which was developed at the Max Planck Institute (MPI) in Hamburg and originated from a model version of the European Centre on Medium Range Weather Forecast (ECMWF). There, the respective variables at each grid point, and at every model level in the case of atmospheric temperature and water vapor, are perturbed by a unit change. The radiative impact is evaluated over a large number of scenes, in our case at every actual two hourly call to radiation for a year. Monthly means are used to retain the annual cycle, and we save all the TOA, surface, longwave, shortwave, clear-sky, and all-sky flux components. The kernels are calculated within the ECHAM6 atmospheric model, which yields consistency between the kernel computations and the studied model. Thereby, we further take advantage of the parallel computational environment, avoiding having to write large amounts of data to disks, facilitating calculations of kernels under different conditions (e.g., different CO_2) and with future updated versions of the model. In the present study, we use kernels calculated with ECHAM6 at T63 horizontal spectral truncation with 47 vertical levels, the atmospheric configuration used in MPI-ESM-LR, but here coupled to a 50 m mixed-layer ocean run to steady state at preindustrial CO_2 (Control simulation (CTRL) with CO_2 concentrations at 284.7 ppmv), at doubled ($2xCO_2$), and at quadrupled concentrations ($4xCO_2$). The resulting all-sky TOA radiative kernels calculated with preindustrial CO_2 presented in Figures 1 and 2 are found to be in qualitative agreement with previous studies [cf. *Soden et al.*, 2008].

[9] The radiative kernels are used to decompose the annual-mean TOA radiation change with respect to the preindustrial state (Equation (1)) into contributions from CO_2, temperature (T), water vapor (W), clouds (C), and surface albedo (A):

$$\Delta R \approx \Delta R_{CO_2} + \Delta R_T + \Delta R_W + \Delta R_C + \Delta R_A. \qquad (2)$$

[10] Then, linear regression with respect to ΔT_s can be applied to obtain each component's contribution to the forcing ($F \approx F_{CO_2} + F_T + F_W + F_C + F_A$) and to the feedback factor ($\lambda \approx \lambda_T + \lambda_W + \lambda_C + \lambda_A$). The direct CO_2 radiative forcing is assumed to be log-linear in the CO_2 concentration [*Arrhenius,* 1896; *Pierrehumbert,* 2011], such that $F_{CO_2} \approx K_{CO_2} \cdot \Delta \log_2(\mathrm{CO}_2)$, where K_{CO_2} is the CO_2 kernel. The surface albedo-induced change in TOA radiation is calculated by averaging $\Delta R_A \approx K_A \cdot \Delta A$ over the year and the globe, where $K_A = \partial R / \partial A$ is the monthly mean surface albedo kernel and ΔA is the change in effective solar-weighted surface albedo, calculated from the monthly mean downwelling and reflected shortwave irradiance at the surface. For water vapor and temperature, it is necessary to vertically integrate the product of

the kernel and the state change, which can in practice be done by summing over the model levels (i), e.g.:

$$\begin{aligned}\Delta R_T &\approx K_{T_s}\cdot\Delta T_s+\int_{p_s}^{0}[K_T\cdot\Delta T]dp\\ &\approx K_{T_s}\cdot\Delta T_s+\sum_{i=1}^{nlev}\left[K_T^i\cdot\Delta T^i\right],\end{aligned}\tag{3}$$

where K_T^i is the per model level mass-weighted temperature kernel and *nlev* is the number of model levels. It is straightforward to separate the stratospheric and tropospheric contributions by summing over the respective domains, and one can separate the Planck response, which is that due to a vertically uniform warming of ΔT_s throughout the troposphere, from the lapse-rate feedback which is due to deviations from vertically uniform tropospheric warming. The water vapor impact on radiation is integrated vertically in the same way, except that the expression is formulated in terms of the natural logarithm of specific humidity.

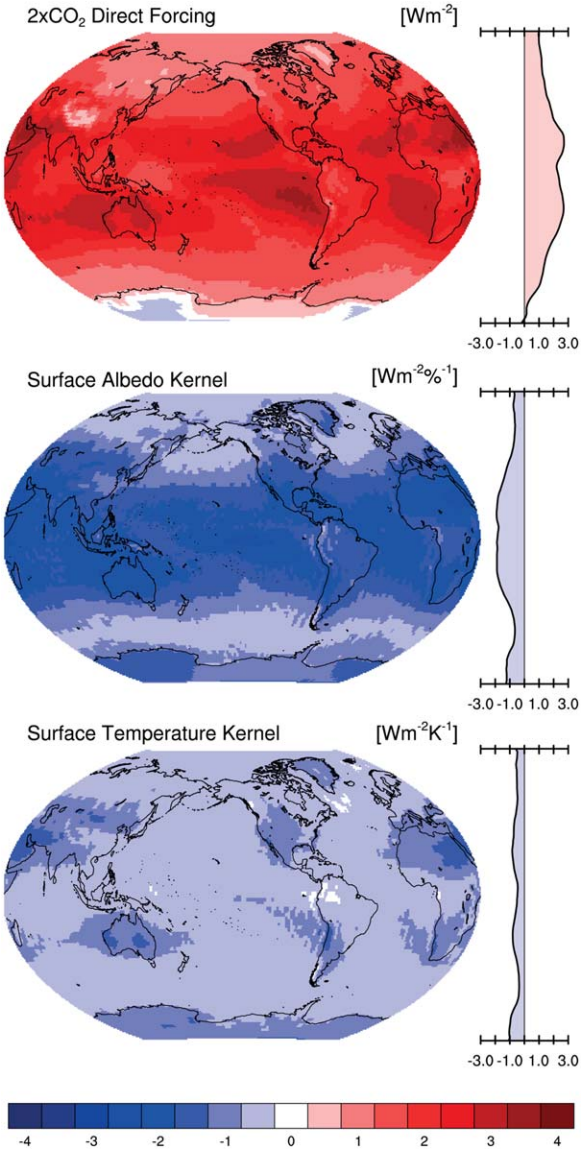

Figure 1. Radiative kernels derived for preindustrial CO_2 conditions. (top) The direct TOA radiative forcing from a doubling of CO_2, (middle) the TOA radiation change with respect to a one percent increase in the surface albedo, and (bottom) the TOA radiation change after an increase of the surface temperature by 1 K. Zonal means are shown to the right of the maps. Positive values indicate energy input in the climate system.

2.2. Correction of the Cloud Feedback Factor for Environmental Masking Effects

[11] Often the change in cloud radiative effect (ΔCRE), which is the all-sky minus the clear-sky TOA irradiance, is used as a surrogate for cloud feedback (recent examples include *Gregory and Webb* [2008] and *Andrews et al.* [2012]. Nevertheless, this approach can be misleading because ΔCRE depends not only on changes in the cloud field but also on changes in the environment [*Colman*, 2003; *Soden et al.,* 2004]. *Shell et al.* [2008] and *Soden et al.* [2008] showed that it is possible to compensate for this environmental masking using the radiative kernels to get a better estimate of the actual cloud-induced impact on the TOA radiation balance:

$$\begin{aligned}\Delta R_C \approx{}&\Delta\mathrm{CRE}-\left(K_{T_s}-K_{T_s}^{clr}\right)\cdot\Delta T_s\\ &-\int_{p_s}^{0}\left[\left(K_T-K_T^{clr}\right)\cdot\Delta T\right]dp\\ &-\int_{p_s}^{0}\left[\left(K_W-K_W^{clr}\right)\cdot\Delta\ln(q)\right]dp\\ &-\left(K_A-K_A^{clr}\right)\cdot\Delta A\\ &-\left(K_{CO_2}-K_{CO_2}^{clr}\right)\cdot\Delta\log_2(\mathrm{CO}_2).\end{aligned}\tag{4}$$

Here, *clr* denotes clear-sky kernels, q is specific humidity and, as in *Shell et al.* [2008], the vertical integration is done over the entire atmosphere.

[12] We used this approach in our computations of the cloud feedback and found a striking difference between ΔCRE and ΔR_C (Figure 3). The contribution to forcing by fast cloud adjustment (F_C, y-axis intercept) is more than doubled (from 0.82 ± 0.03 to 1.97 ± 0.03 W m^{-2}) by compensating for environmental masking, mainly due to absorption by CO_2 (1.33 W m^{-2}). Further, there is a shift from a statistically insignificant slope in ΔCRE (0.11 ± 0.11 W m^{-2} K^{-1}), to a clearly positive slope in ΔR_C in the second part of the regression after applying Equation (4), yielding a positive cloud feedback factor λ_C of 0.62 ± 0.09 W m^{-2} K^{-1}. The cloud masking correction terms pertaining to water vapor and surface albedo both increase in a warming climate, while increasing temperatures act to reduce the estimate of the cloud feedback. These findings show that a correction for environmental masking is essential when studying the cloud feedback.

2.3. State Dependency of Radiative Kernels

[13] The application of the radiative kernels is in principle limited to only small perturbations to climate,

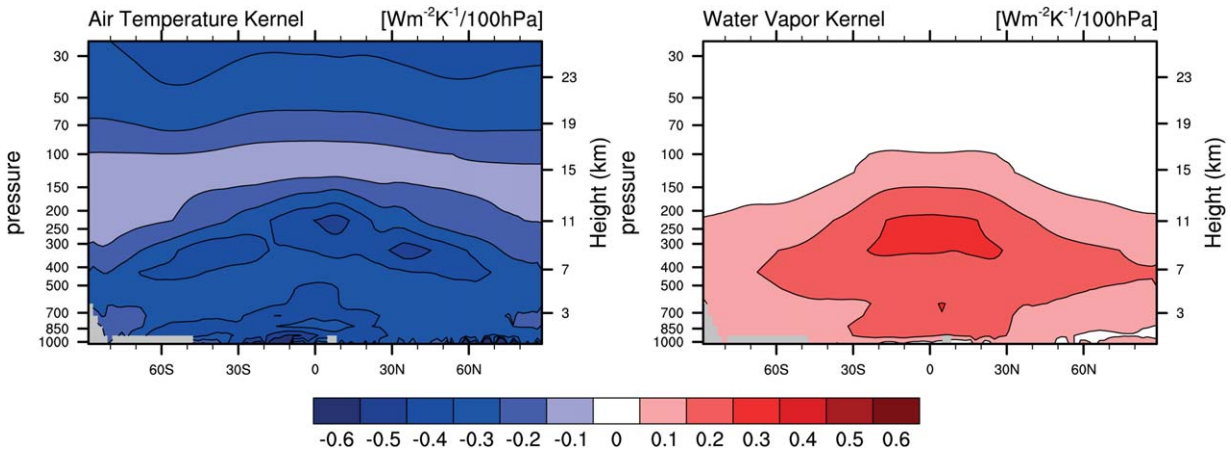

Figure 2. Radiative kernels derived for preindustrial CO_2 conditions. (left) The zonal-mean TOA change in radiation with respect to a 1 K warming of the atmospheric temperature at different heights of the atmosphere. (right) The radiation change induced by an increase in atmospheric water vapor corresponding to a 1 K warming at fixed relative humidity. Positive values indicate energy input in the climate system.

because the derivatives of TOA radiation with state change depend on the climate mean state [*Jonko et al.*, 2012]. Indeed, the shifts in the radiative kernels between the preindustrial and quadrupled CO_2 steady states are appreciable (Figure 4). For a 1 K vertically uniform warming more infrared radiation is emitted directly from atmosphere, at the expense of radiation from the surface, while the associated radiative impact of increasing water vapor is enhanced. The impacts of surface albedo reductions due to melting snow and ice in the Arctic and Southern Ocean are weakened in a warmer climate, almost exclusively due to thickening clouds in these regions (not shown). In the central Arctic, the surface albedo kernel is reduced to only half of the preindustrial value in the warmer climate. Finally, the direct radiative impact of doubling CO_2 increases in the warmer climate uniformly by nearly 1 W m^{-2}. As will be shown in section 3.5, these state dependencies in the radiative kernels have far-reaching consequences for the interpretation of the results of kernel-based feedback analyses.

2.4. Comparison to PRP and Model Response

[14] We benchmark our radiative kernel methodology using both the preindustrial state (CTRL) kernel and the $2xCO_2$-state kernel, against the full model response and feedback factors estimated by the partial radiation perturbation method (PRP), which was introduced by *Wetherald and Manabe* [1988] and *Colman and McAvaney* [1997]. The two-sided PRP-method to which we compare here (Table 1) is described by *Klocke et al.* [2013]. The validation is done here with ECHAM6 coupled to a mixed-layer ocean (MLO) run to stationarity with $2xCO_2$. There is, in general a good agreement between feedback factors estimated from the two methods. Temperature, cloud, and surface albedo feedbacks are slightly stronger when estimated using kernels, while water vapor feedback is weaker than the PRP estimate when computed with the CTRL-kernel and stronger when evaluated with the 2xCO2-state kernel. The kernel-derived total feedback, which is the sum of the individual feedbacks, is stronger, i.e., more negative, than the actual model feedback (-1.19 W $m^{-2}K^{-1}$) which is based on TOA radiative fluxes, with both PRP (-1.28 W m^{-2} K^{-1}) and CTRL-kernel (-1.29 W m^{-2} K^{-1}). The $2xCO_2$-kernel-derived estimate yields a smaller feedback factor (-1.09 W m^{-2} K^{-1}) than the model estimate. Comparing the kernel estimated total radiation imbalance (ΔR) to the imbalance resulting directly from the model we find that the estimate based on the CTRL-kernel fares best.

3. Results

[15] In what follows, we perform a regular Gregory analysis and discuss the nonlinearity of the MPI-ESM-LR coupled climate model. Then, the magnitude and spatial structure of the individual feedbacks and fast adjustments is assessed using the combined Kernel-Gregory method and the ability to quantify them from idealized experiments with prescribed sea surface temperatures (SSTs) is investigated. Finally, we explore which feedbacks contribute to the nonlinear behavior of the model.

3.1. Gregory Analysis

[16] A Gregory analysis of the 150 year long MPI-ESM-LR abrupt $4xCO_2$ simulation is presented in Figure 5, where the TOA radiation imbalance is regressed on the surface temperature change. The various regressed feedback factors and intercepts are listed in Table 2. The model exhibits a relatively large adjusted forcing of 9.15 W m^{-2}, which is substantially above twice the canonical value of 3.7 W m^{-2} for a single doubling of CO_2 including only stratospheric adjustment [*Forster et al.,* 2007; *Stuber et al.,* 2001; *Hansen et al.,* 1997]. The MPI-ESM-LR extrapolated equilibrium climate sensitivity of 7.46 K with respect to $4xCO_2$ is in the middle of the range of the Coupled Model

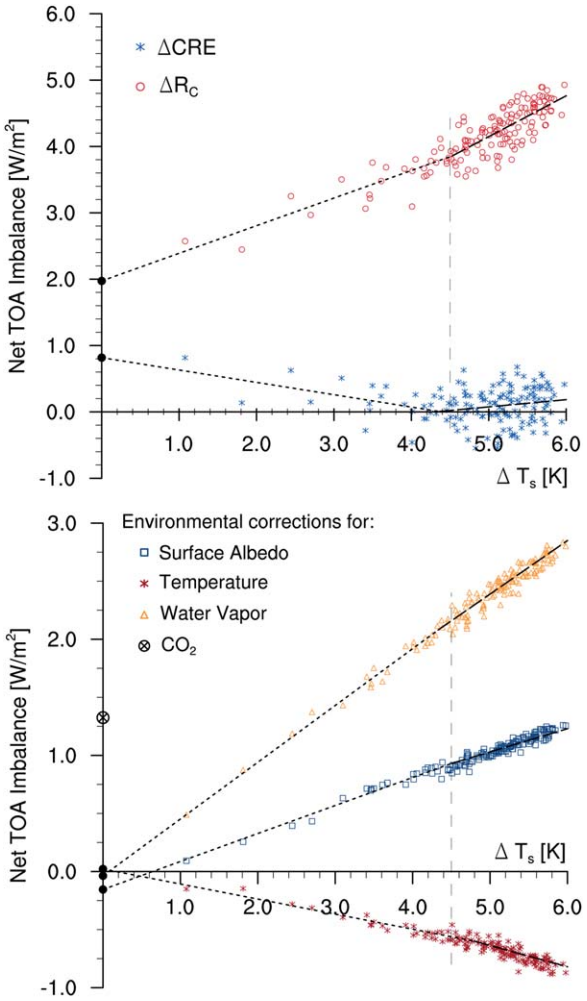

Figure 3. (top) A comparison of the change in ΔCRE to the corrected ΔR_C following Equation (4) in MPI-ESM-LR after abruptly quadrupling CO_2. Regressions on the global mean surface temperature change are made on the first 20 and last 130 years separately. Black dots are extrapolated values. Positive values indicate energy input in the climate system. (bottom) Corresponding environmental correction terms (Equation (4)) for temperature, water vapor, surface albedo, and CO_2.

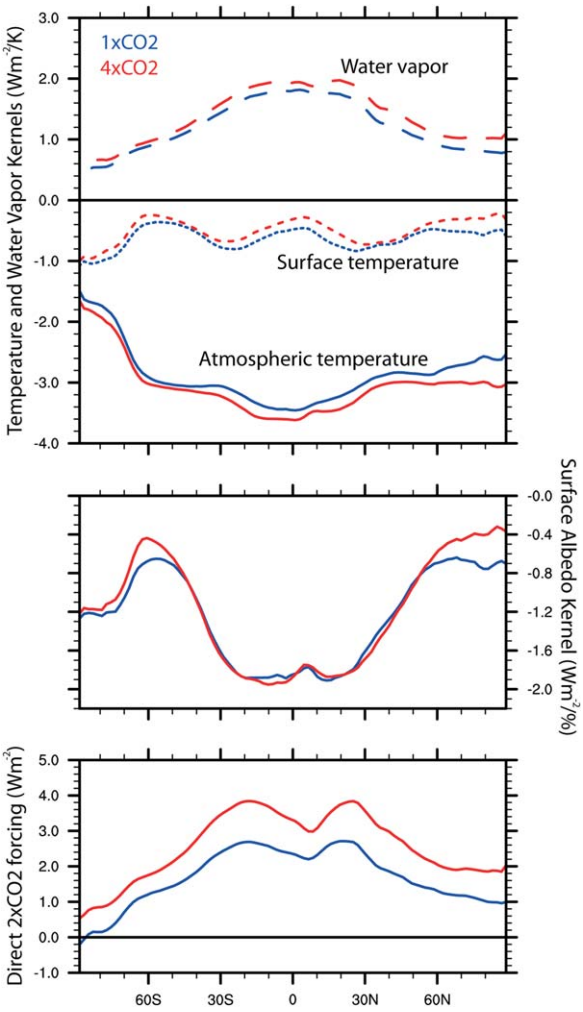

Figure 4. Vertically integrated and zonally averaged radiative kernels for preindustrial (blue) and quadrupled CO_2 (red) conditions. (top) Both the temperature and water vapor kernels are with respect to a uniform 1 K warming and, for water vapor, with fixed relative humidity. (middle) The TOA radiation change with respect to 1% increase in surface albedo. (bottom) The direct TOA forcing from a doubling of CO_2 (blue indicates the doubling from 1x to 2xCO_2 and red indicates the doubling from 4x to 8xCO_2), without including atmospheric adjustments. Positive values indicate energy input in the climate system.

Intercomparison Project (CMIP) Phase 5 climate models [*Taylor et al.,* 2012; *Andrews et al.,* 2012].

[17] A distinct feature of the MPI-ESM-LR, and several other coupled climate models, is the nonlinear relation between radiation imbalance and global mean surface temperature following an abrupt quadrupling of CO_2 [*Andrews et al.*, 2012]. To assess this nonlinearity we—somewhat arbitrarily—make separate regressions on the first 20 years and the last 130 years as suggested by *Stevens et al.* [2013]; our overall conclusions are insensitive to this choice. The piecewise linearly regressed effective climate sensitivity proportional to $-1/\lambda$, increases by about 60% as λ drops from -1.44 to -0.90 W m^{-2} K^{-1} after 20 years. The change in slope is statistically significant at the 95% confidence level (Table 2). Mean values of 30 year 4xCO_2 simulations with prescribed sea surface temperatures, such as sstClim 4xCO_2, Atmospheric Model Intercomparison Project (AMIP) 4xCO_2, and MLO 4xCO_2 (open symbols), fall on the regression line and thus support the steeper initial slope.

[18] If the underlying cause of the nonlinearity is a decadal adjustment associated with differential warming patterns of the ocean associated with deep ocean heat uptake [*Winton et al.*, 2010], then one expects that the regressed feedback factors depend only on the time since the applied forcing, and not on the forcing

Table 1. Feedback factors λ (W m^{-2} K^{-1}) and TOA radiation imbalance ΔR (W m^{-2}), evaluated on the last 12 years of the MLO run with 2xCO2 compared to the control MLO run[a]

	λ_T	λ_W	λ_C	λ_A	λ	ΔR
From Model					−1.19[b]	0.12
PRP Method	−4.05[c]	1.98	0.63[b]	0.16	−1.28[b]	
CTRL-Kernel	−4.18[c]	1.94	0.72[b]	0.23	−1.29[b]	−0.06
2xCO2-Kernel	−4.19[c]	2.13	0.78[b]	0.19	−1.09[b]	1.11

[a]The kernel-derived estimates are shown in comparison to the more accurate two-sided PRP method, where the values are taken from Table 2 in *Mauritsen et al.* [2013]. The total feedback factors for both estimates result from the sum of their individual contributions, whereas the total model feedback factor is based on model TOA radiation fluxes.

[b]Both λ_C and λ include contributions from fast cloud adjustments. Hence, the cloud feedback is more positive than the true temperature-dependent cloud feedback. Please note, that *Mauritsen et al.* [2013] use the 2 m air temperature for their feedback analysis, whereas we use the surface temperature. This leads to about 5% larger feedback factors in our case.

[c]λ_T is here only evaluated over the troposphere.

strength or temperature change. Indeed, when we apply a forcing of 2xCO$_2$ to MPI-ESM-LR the slopes before and after year 20 are statistically indistinguishable from those of the 4xCO$_2$ run (Figure 5 and Table 2), although it should be noted that internal variability introduces additional statistical uncertainty when the model is forced weakly. Here again, the average of a 30 year long experiment with 2xCO$_2$ and prescribed SST (open symbol) falls on the first regression line and therefore supports the steeper initial slope of the coupled run.

[19] What matters in the end, however, is the equilibrium climate sensitivity (S). The coupled model run with 4xCO$_2$ exhibits an extrapolated sensitivity ($S = 7.46$ K) that is more than twice that of the 2xCO$_2$ run ($S = 3.49$ K). The difference is, however, not statistically significant as the model is far from equilibrated with the applied forcings at the end of the runs. When instead coupled to a mixed-layer ocean the model reaches stationarity after about two decades, thus yielding a more certain estimate of S. It should be noted that we do not

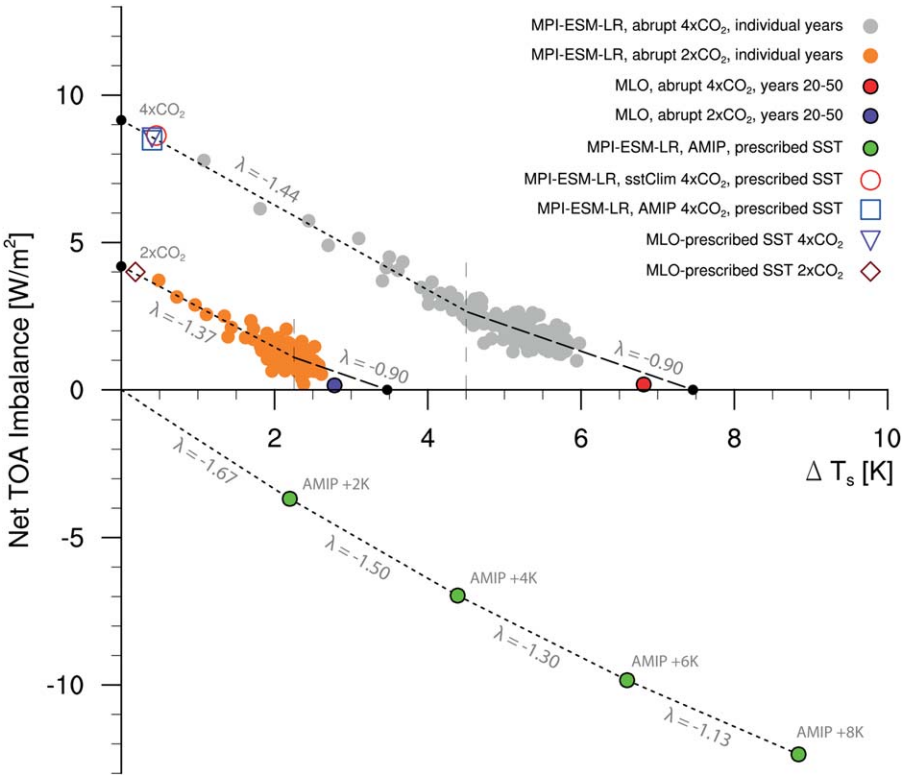

Figure 5. Relation between TOA radiation imbalance and surface temperature change in a set of experiments with the coupled MPI-ESM-LR model, with prescribed SSTs, and using a mixed-layer ocean (MLO). Only global, annual means are used. Black dots indicate extrapolated values. Dashed and dotted lines are used for separate regressions, respectively. For the MPI-ESM-LR abrupt 4xCO$_2$ experiment, the regressions are done for the first 20 and the last 130 years, respectively, which is approximately above and below 4.5 K warming. For the MPI-ESM-LR abrupt 2xCO$_2$ experiment, the regressions are done for the first 20 and last 80 years, respectively, which approximately above and below 2.25 K warming. The sstClim 4xCO$_2$ experiment uses prescribed SSTs from the preindustrial MPI-ESM-LR coupled model. The value presented here is a 30 year mean. The AMIP experiments use prescribed SSTs from observations. The values shown here are 30 year means. The MLO-prescribed SST experiments use SSTs from the unperturbed MLO run. Positive values indicate energy input in the climate system.

Table 2. Values of total adjusted CO_2 forcing F (W m^{-2}), total feedback factor λ (W m^{-2} K^{-1}), and effective climate sensitivity S (K), based on radiative fluxes at the TOA[a]

Experiment	F	λ	S
MPI-ESM-LR abrupt 4xCO₂			
Years 1–20	9.15 ± 0.05	−1.44 ± 0.17	6.34 −0.7/+0.9
Years 21–150	6.69 ± 0.04	−0.90 ± 0.13	7.46 −1.0/+1.3
MPI-ESM-LR abrupt 2xCO₂			
Years 1–20	4.19 ± 0.06	−1.37 ± 0.27	3.05 −0.5/+0.8
Years 21–100	3.13 ± 0.15	−0.90 ± 0.36	3.49 −1.1/+2.7
MLO, Years 20–49			
abrupt 4xCO₂			6.82 ± 0.03
abrupt 2xCO₂			2.78 ± 0.03
AMIP, 30 years			
AMIP + 2 K		−1.67 ± 0.18	2.20 ± 0.07
AMIP + 4 K		−1.59 ± 0.08	4.39 ± 0.08
AMIP + 6 K		−1.49 ± 0.05	6.60 ± 0.08
AMIP + 8 K		−1.40 ± 0.04	8.84 ± 0.08

[a]For MPI-ESM-LR, F and S are extrapolated values since the simulations have not been run into equilibrium. For the AMIP and MLO experiments, S is a mean value of 30 years. For all values, the 95% confidence intervals are given.

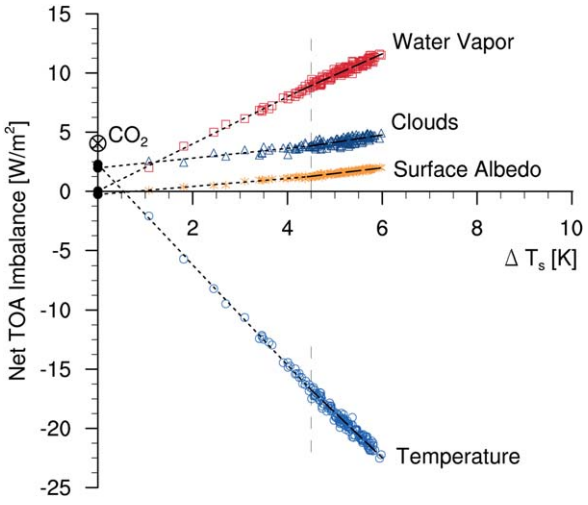

Figure 6. Decomposition of the net TOA radiation imbalance into individual contributions in the MPI-ESM-LR experiment with abruptly quadrupled CO_2 calculated using the CTRL-state radiative kernels. In all cases, linear regressions are made on the first 20 and last 130 years, respectively. The corresponding values are listed in Table 3. Black dots represent extrapolated values and indicate fast adjustments. Positive values indicate energy input in the climate system.

expect the absolute climate sensitivity to be the same in the coupled and MLO models, owing to different base-state SST-patterns [*Dommenget*, 2012]. We obtain 2.78 K warming from the 2xCO_2 run (average of years 20–49), and about 6.82 K warming for 4xCO_2, i.e., 45% higher S for the second doubling compared to the first doubling with respect to preindustrial conditions. This suggests that decadal ocean adjustments is not the only source of nonlinearity, as the MLO setup does not include a deep ocean circulation and still exhibits increasing S.

[20] The increasing S could also be due to state dependencies in the underlying feedback mechanisms. Support for this idea is found in AMIP simulations with uniformly increased SSTs, so-called Cess experiments [*Cess*, 1990]. Here, indeed λ changes from −1.59 W m^{-2} K^{-1} between present day and +4 K uniform warming to −1.21 W m^{-2} K^{-1} between the AMIP +4 K and AMIP +8 K run (Table 2). Note that the magnitudes of the total feedback factors may differ compared to the coupled model owing to the somewhat artificial uniform warming pattern [*Gettelman et al.*, 2012].

[21] While the presented analysis is insufficient to point at or rule out one or the other explanation for the nonlinear behavior of the MPI-ESM-LR model, it is clear that the impacts are nonnegligible for future CO_2-forced climate scenarios [*Moss et al.*, 2010] and that a refined view of climate sensitivity is needed.

3.2. Combined Kernel-Gregory Feedback Analysis

[22] We apply the radiative kernels to the fully coupled simulation with the CO_2 concentration abruptly quadrupled in order to decompose the impact on radiation imbalance relative to the unperturbed state and regress the TOA radiation imbalance of each feedback variable against the global mean surface temperature change in order to determine fast adjustments and feedback factors (Figure 6 and Table 3).

[23] The TOA radiation budget is initially offset by three main contributions: the direct CO_2 forcing (50%) and two indirect forcings by fast adjustments in temperature (28%) and clouds (24%). Since the fast cloud adjustment has not been considered in many climate forcing studies so far [*Forster et al.*, 2007; *Stuber et al.*, 2001; *Hansen et al.*, 1997], this contribution might be an explanation for the relatively large total adjusted forcing of 9.15 W m^{-2} found in the model. Here, the temperature impact on radiation is calculated over the entire atmosphere, and thus includes both, a fast adjustment primarily in the stratosphere, and the feedback from slow global warming. Fast adjustments from water vapor and surface albedo are, although statistically significant based on the linear regression, so small that these components could be considered "classical" surface temperature-dependent feedbacks in good agreement with findings by *Colman and McAvaney* [2011]. However, the small negative contribution to forcing we find here from surface albedo turns out to be an artifact of applying linear regression (section 3.4).

[24] As the global mean surface temperature rises, the large negative temperature and positive water vapor feedbacks dominate the evolving TOA radiation budget with smaller positive contributions from cloud and surface albedo feedbacks.

3.3. Spatial Structure of Feedbacks

[25] Maps of feedback factors and adjustments can be obtained by regressing the local kernel-derived radiation imbalance on the global mean surface temperature

Table 3. Values of feedback factors λ (W m^{-2} K^{-1}) derived by the combined Kernel-Gregory analysis for each component and their sum, as well as forcings F (W m^{-2}), either directly from CO_2 or from fast adjustments which are determined by extrapolation.[a]

Experiments	CO_2	Temperature	Water Vapor	Clouds	Surf. Albedo	Sum
MPI-ESM-LR abrupt 4xCO_2, 150 years						
CTRL-Kernel, F (From Years 1–20)	4.05	2.28 ± 0.04	0.03 ± 0.02	1.97 ± 0.03	−0.27 ± 0.003	8.07 ± 0.09
CTRL-Kernel, λ (Years 1–20)	0	−4.23 ± 0.15	1.99 ± 0.10	0.42 ± 0.13	0.34 ± 0.04	−1.49 ± 0.42
CTRL-Kernel, λ (Years 21–150)	0	−3.83 ± 0.13	1.79 ± 0.08	0.62 ± 0.09	0.48 ± 0.03	−0.94 ± 0.33
MPI-ESM-LR abrupt 4xCO_2, 150 years						
4xCO_2-Kernel, F (From Years 1–20)	5.03	2.97 ± 0.05	0.03 ± 0.03	1.95 ± 0.03	−0.10 ± 0.001	10.60 ± 0.11
4xCO_2-Kernel, λ (Years 1–20)	0	−4.30 ± 0.17	2.48 ± 0.13	0.54 ± 0.14	0.19 ± 0.03	−1.09 ± 0.47
4xCO_2-Kernel, λ (Years 21–150)	0	−3.90 ± 0.15	2.23 ± 0.10	0.78 ± 0.10	0.27 ± 0.02	−0.62 ± 0.37
MLO, abrupt 4xCO_2, 50 years						
CTRL-4xCO_2-Mean Kernel, F	5.03	2.42 ± 0.02	−0.26 ± 0.01	1.89 ± 0.02	−0.36 ± 0.001	8.72 ± 0.05
CTRL-4xCO_2-Mean Kernel, λ	0	−4.02 ± 0.07	2.03 ± 0.06	0.48 ± 0.07	0.31 ± 0.02	−1.20 ± 0.22
MLO, abrupt 2xCO_2, 50 years						
CTRL-Kernel, F	2.02	1.42 ± 0.03	−0.48 ± 0.01	0.66 ± 0.04	0.05 ± 0.001	3.67 ± 0.08
CTRL-Kernel, λ	0	−4.13 ± 0.14	1.97 ± 0.10	0.49 ± 0.16	0.23 ± 0.03	−1.44 ± 0.43
AMIP + 4K − AMIP, 30 years-mean						
CTRL-4xCO_2-Mean Kernel, λ	0	−4.44 ± 0.15	2.21 ± 0.08	0.59 ± 0.04	0.08 ± 0.01	−1.55 ± 0.28
AMIP + 8K − AMIP + 4K, 30 years-mean						
CTRL-4xCO_2-Mean Kernel, λ	0	−4.49 ± 0.19	2.30 ± 0.10	0.79 ± 0.06	0.09 ± 0.01	−1.31 ± 0.36

[a]For MPI-ESM-LR fully coupled experiments piecewise linear regressions are done for the first 20 years and the following 130 years and estimates computed with the CTRL-state kernel as well as with the 4xCO_2-state kernel are shown. The results can be compared with results from the MLO and AMIP experiments. For each of those feedback analyses the best kernel estimate is used, which is indicated in the table. For the AMIP experiments, the feedback factors are calculated using 30 year time means. For all values, the 95% confidence intervals are given.

change. The spatial structures of feedback factors in the MPI-ESM-LR model (Figure 7) are qualitatively similar to the CMIP3 multimodel mean [cf. *Soden et al.*, 2008]. Both water vapor and temperature feedbacks are relatively smooth with maxima in the tropics. The temperature feedback has a second maximum in the Arctic because there the temperature change is more pronounced. Cloud feedback is rich in structure, with positive contributions in the tropics and subtropics dominating over negative contributions in the Southern Ocean and the Arctic Ocean. The positive feedbacks in the tropics mainly result from positive longwave cloud feedback, peaking in the west Pacific (not shown). This feature is in agreement with the fixed anvil temperature (FAT) hypothesis from *Hartmann and Larson* [2002] that the temperature emission of tropical anvil clouds stays nearly constant during climate change, constituting a positive longwave cloud feedback. Surface albedo feedback is dominated by sea ice loss, with small contributions from snow melt on land and vegetation change. The temperature feedback is dominated by the Planck feedback which is the change in emitted longwave energy throughout the troposphere associated with the amount of surface temperature change. The lapse-rate feedback describing the change in emitted longwave energy associated with a change in lapse rate, is negative in most of the tropics and midlatitudes, except in parts of the continents where the surface warms faster than the atmosphere. In the Arctic, the lapse-rate feedback is generally positive because of the strong surface-based warming.

[26] By comparing the feedback factors derived from the coupled simulation with those from runs with uniformly increased SSTs (AMIP +4K, Figure 8) the suitability of the Cess-type experiment for studying feedbacks and feedback changes as seen in Figure 5 can be assessed. The comparison reveals qualitative similarities in the temperature, water vapor, and cloud feedbacks. The small structural differences compared to the coupled simulation probably result from differences in the SST change patterns and the mean climate state [*Gettelman et al.*, 2012]. Surface albedo feedback is naturally weaker because sea ice is prescribed in this idealized run, and so only vegetation and snow on land can respond to the warming. There is little correspondence in the vertically integrated lapse-rate feedback between the two simulations which can, besides the above named reasons, also be due to the absence of CO_2 forcing. However, the qualitative agreement in spatial structure with the coupled model shows that the Cess experiment is in general suitable for studying temperature, water vapor, and cloud feedbacks, although the quantitative agreement could be better.

3.4. Spatial Structure of Fast Adjustments

[27] We focus next on fast adjustments to quadrupled CO_2 obtained from extrapolation of regressions on the first 20 years (Figure 9). We find positive global-mean

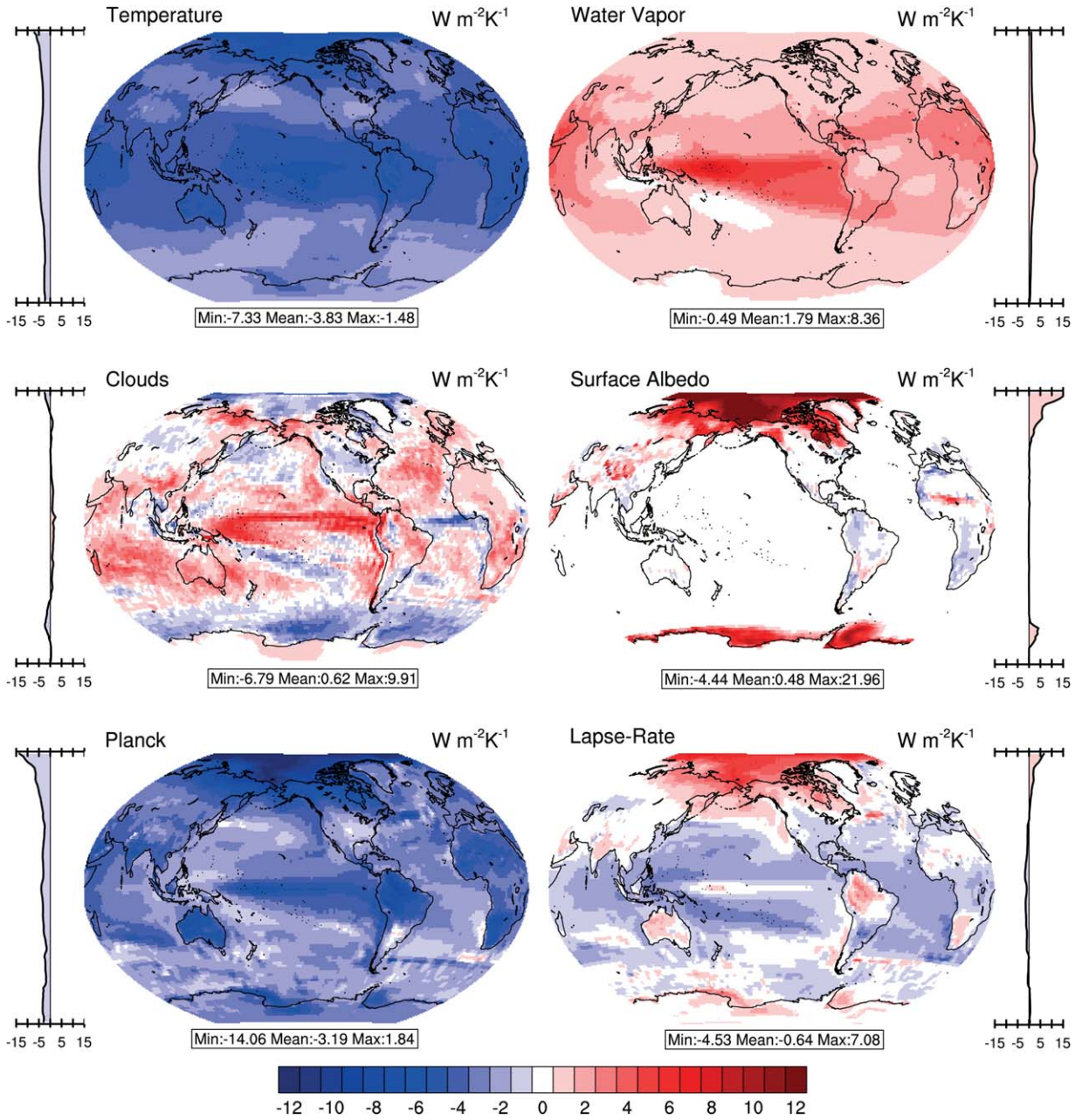

Figure 7. Maps of feedback factors obtained using the CTRL-state radiative kernels on years 21–150 of the simulation with MPI-ESM-LR with abruptly quadrupled CO_2. Note that using the CTRL-state kernel on a warm climate exaggerates the surface albedo feedback (Figure 4). The bottom two plots are a decomposition of the temperature feedback factor into the Planck feedback, which is a vertically uniform warming, and the lapse-rate feedback, which is due to deviations from the uniform warming. Both of which are evaluated over the troposphere only. Zonal means are shown next to the maps. Positive values indicate energy input in the climate system.

contributions from temperature and clouds, near zero from water vapor, and a weakly negative contribution from surface albedo. The temperature adjustment is dominated by the well-known positive stratospheric adjustment. However, nonnegligible negative tropospheric temperature adjustment occurs especially over land in the northern hemisphere. This results from a faster surface warming over land than over ocean relative to the global mean surface temperature change. The cloud adjustment is again rich in structure, probably here in part due to noise owing to the extrapolation. It is generally stronger over land than over the oceans. The water vapor adjustment is small in the global mean due to spatial cancellation. The signal seen over Indonesia could be influenced by the system state at the time of applying the abrupt forcing.

[28] By comparing with the sstClim 4xCO_2 experiment (Figure 10), it is possible to see whether the results

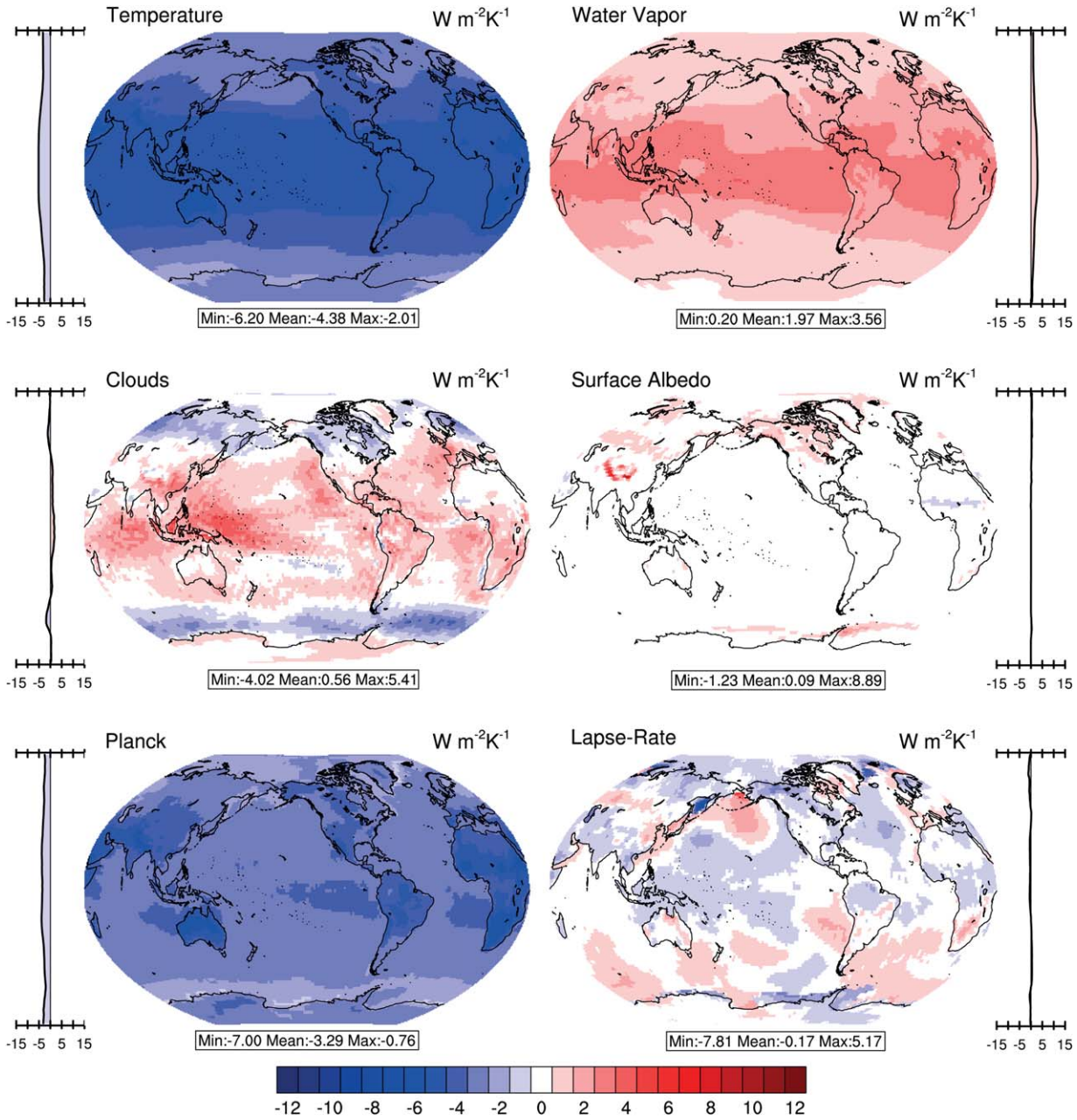

Figure 8. Maps of feedback factors obtained using the CTRL-4xCO_2-average radiative kernels on AMIP +4K run. The Planck and lapse-rate feedbacks are evaluated over the troposphere only. Zonal means are shown next to the maps. Positive values indicate energy input in the climate system.

estimated from regressions in the coupled model are comparable to estimates by 30 year means in a model configuration with SSTs prescribed from the coupled model. We find qualitative agreement in the temperature and cloud adjustments. The negative tropospheric temperature adjustment is stronger, probably because land temperatures are given time to warm in response to the CO_2 increase. Clouds exhibit positive adjustment over land, tropical, and subtropical oceans, while the storm-track regions in both hemispheres indicate negative adjustment. The slight positive adjustment in surface albedo in the sstClim 4xCO_2 simulation is likely due to melting snow, associated with land warming.

[29] The negative sea ice albedo adjustment in the coupled model appears unphysical, as it is difficult to imagine a process whereby sea ice becomes more reflective with increasing CO_2. The contribution to radiation from surface albedo change increases nonlinearly exhibiting a delayed response relative to the global mean temperature (Figure 11). This delay could be due to a

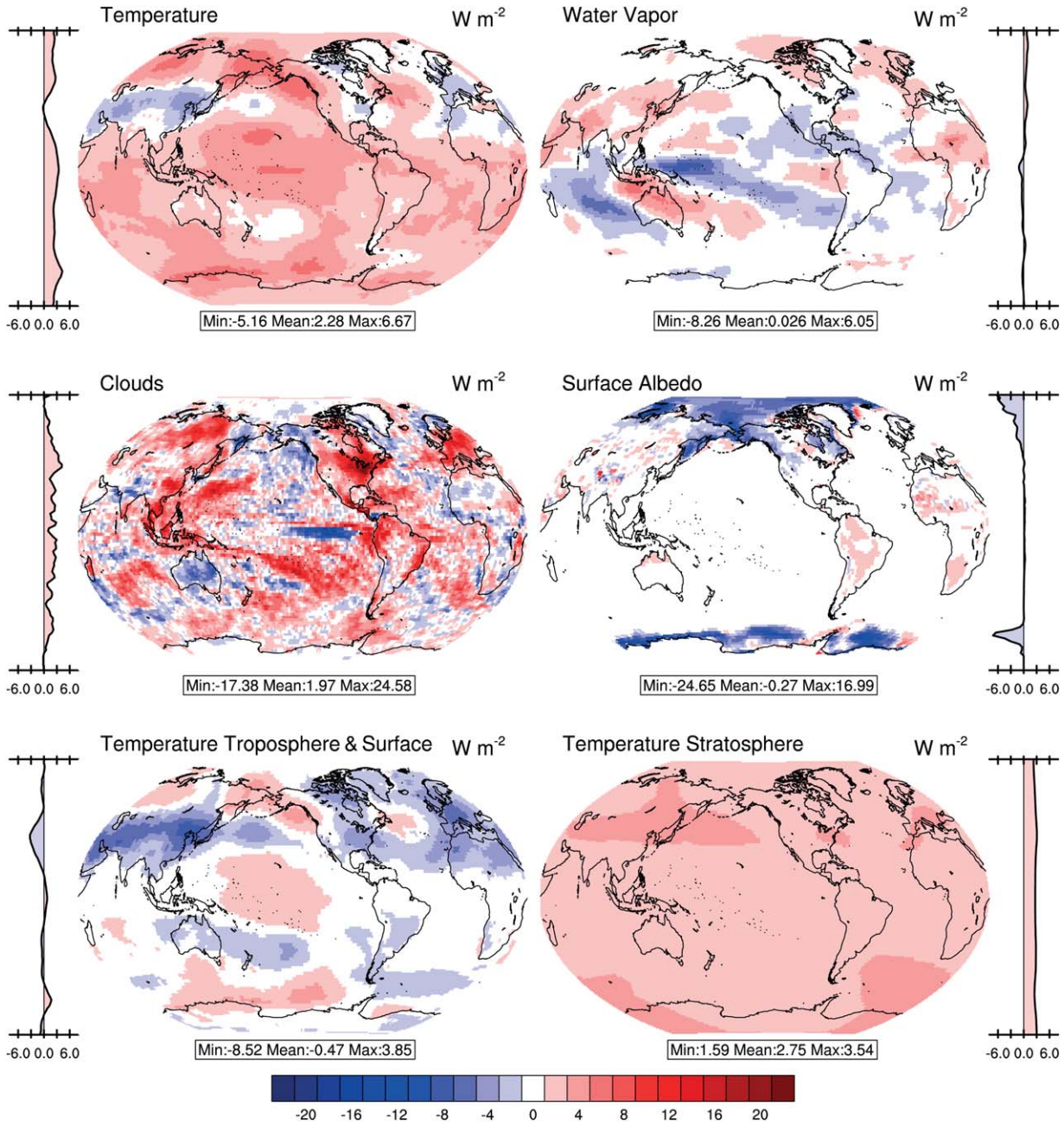

Figure 9. Fast adjustments from the MPI-ESM-LR coupled simulation with abruptly quadrupled CO_2 (MPI-ESM-LR abrupt 4xCO_2) determined from the *y* intercepts of linear regression on years 1–20 using the CTRL-state kernel. Zonal means are shown next to the maps. Positive values indicate energy input in the climate system.

lagged ocean response, and/or an effect of the geometry of the Arctic Ocean coastlines [*Eisenman et al.*, 2011]. Thus, this feature could just be an artifact of applying a linear regression. Another explanation could be the overestimated CTRL-state albedo kernel (section 2.3) contributing to a steeper slope of the albedo-induced radiation imbalance (Figure 11). Using the 4xCO2-state kernel produces less increasing slopes resulting in a smaller absolute value of the y-intercept. Furthermore, the surface albedo radiative impact computed with sstClim 4xCO2 and AMIP 4xCO2 simulations provide no support for a negative surface albedo adjustment. They even show slightly positive values likely owing to melting snow, associated with surface warming. In conclusion, we suggest that surface albedo, like water vapor, exhibits no appreciable adjustment to CO_2 forcing. Further, this artifact in fast adjustment is partly causing an overestimation of the surface albedo feedback in the first two decades of the coupled run.

3.5. Contributing Factors to the Increase of Effective Climate Sensitivity

[30] We are now in a position to explore the change in total feedback factor found to occur after 20 years,

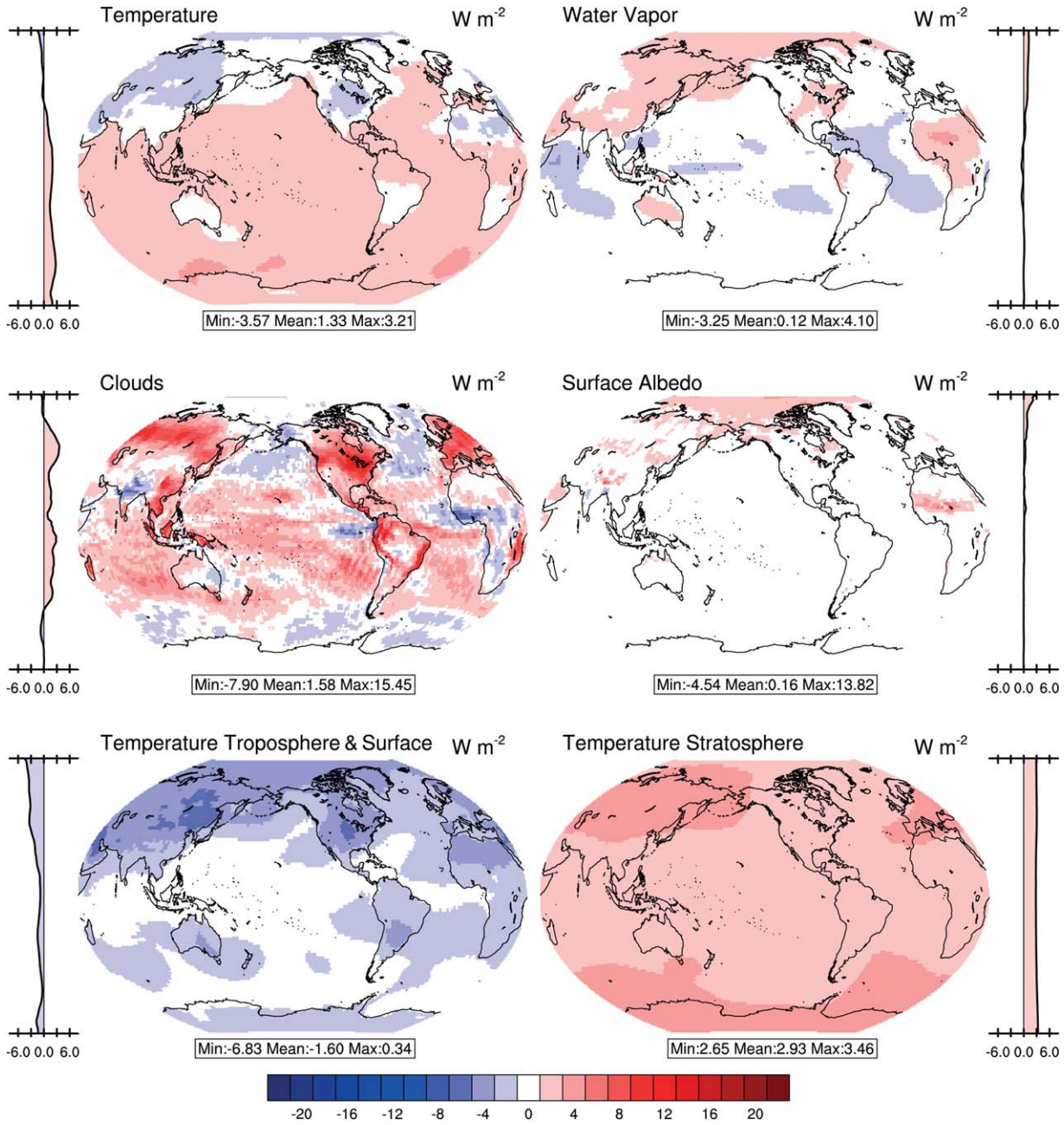

Figure 10. Estimates of fast adjustments from the MPI-ESM-LR coupled simulation with prescribed SSTs and quadrupled CO_2 (sstClim 4xCO_2) calculated using the CTRL-state kernel. Zonal means are shown next to the maps. Positive values indicate energy input in the climate system.

around 4–5 K warming (Figure 5). In order to do that, we first need to investigate how well the kernel-derived estimate represents the change in total feedback directly inferred from the model. Figure 12 shows that the CTRL-state kernel-derived radiation budget, which is computed from the sum of all individual feedbacks (Table 3), reproduces a shift in slope that is most similar to that exhibited by the model. The CTRL-state kernel-derived radiation budget is underestimated by about 1 W m^{-2}, while the slopes match those of the model's TOA radiation budget almost perfectly. Applying the warm-state 4xCO_2 kernels instead, the TOA radiation budget is generally overestimated while the total feedback is underestimated, yielding an overestimation of effective climate sensitivity. The ability of the CTRL-kernel to reproduce the slopes of the model radiation budget is, however, lending itself to compensating errors as can be inferred from maps of the kernel-derived TOA radiation budget change (Figure 13). Although there is a generally good agreement in

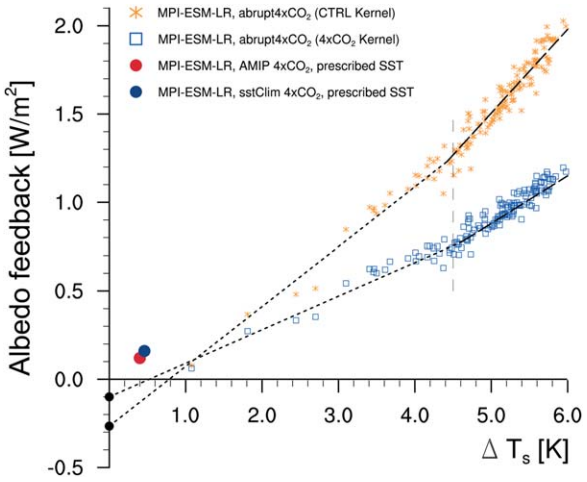

Figure 11. Surface albedo feedback in the MPI-ESM-LR coupled simulation with quadrupled CO_2 (MPI-ESM-LR abrupt $4xCO_2$) computed using the CTRL-state kernel and the $4xCO_2$-state kernel. Linear regressions are done for the first 20 years and the last 130 years of simulation, respectively. Black dots are extrapolated values which indicate fast adjustments. Furthermore, surface albedo adjustments from 30 year means of the AMIP $4xCO_2$ and sstClim $4xCO_2$ experiments are included.

the spatial structure in the model-budget change compared to that estimated using the CTRL-kernel, there is a systematic difference in the Arctic region where the change in radiation is overestimated, while elsewhere the change in radiation is slightly underestimated.

[31] For any given kernel, either in the CTRL or $4xCO_2$ climate, there is a weakening of the negative temperature feedback factor by $+0.40$ W m^{-2} K^{-1} in the last 130 years relative to the first 20 years (Table 3).

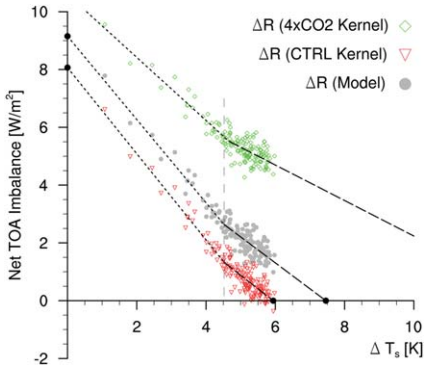

Figure 12. Comparison of the sum of the kernel-derived contributions using the CTRL-state and the $4xCO_2$-state kernels, to the model's net TOA radiation imbalance. In all cases, linear regressions are made on the first 20 and last 130 years, respectively. Black dots are extrapolated values. The corresponding values are listed in Tables 2 and 3.

Likewise, the positive cloud feedback and surface albedo feedback increase in magnitude by $+0.20$ W m^{-2} K^{-1} and $+0.14$ W m^{-2} K^{-1}, respectively, while the water vapor feedback decreases in magnitude by 0.20 W m^{-2} K^{-1} when applying the CTRL-state kernel. One could argue that the CTRL-state kernel is more relevant during the first 20 years and the 4xCO2 kernel is better applicable to the warmer part of the simulation because the derivatives would then be evaluated closer to the current state. Under this assumption, we find instead that water vapor feedback increases, and surface albedo feedback decreases, while temperature and cloud feedback make the total feedback more positive, regardless of the choice of kernels. The changes in the individual feedbacks could be compared to those computed by *Jonko et al.* [2013], who also used the kernel technique to evaluate the change in feedbacks for three successive CO_2 doublings in a fully coupled general circulation model. In agreement with our results, they also find a slightly decreasing temperature feedback and an increasing cloud feedback for their first two CO_2 doublings from preindustrial levels. The water vapor feedback is clearly increasing, but in contrast to our results, their surface albedo feedback is decreasing.

[32] Inspecting the spatial structure of the shift in feedback based on the model's TOA fluxes ($\Delta\lambda$) sheds more light on the causes for the change in feedback with time (Figure 14). Of the $+0.55$ W m^{-2} K^{-1} in total feedback shift, $+0.13$ W m^{-2} K^{-1} comes from the relatively small Arctic region north of 60°N, the Southern Ocean and Antarctica south of 50°S counteracts this by -0.07 W m^{-2} K^{-1}, while the larger region between 50°S and 60°N contributes the most by $+0.49$ W m^{-2} K^{-1}. These results show that in the MPI-ESM-LR coupled model, the change in total feedback does not result from a delayed response of the Southern Ocean as was suggested by *Senior and Mitchell* [2000]. Here, the Southern Ocean actually counteracts the increase in effective climate sensitivity. Comparing the shift of the model total feedback to the kernel-derived estimate (Figure 14, top right) shows the ability of the kernel technique to replicate the feedback change on spatial scale. The difference is dominated by an overestimate of the surface albedo feedback in the Arctic region by the kernel technique, where the error is as large as the actual signal. This overestimation is probably due to the change in surface albedo kernel with climate state (Figure 4). Given the structure of the individual feedback mechanisms, it appears however that the surface albedo feedback in the Arctic does contribute positively to the shift in climate sensitivity, although not as much as indicated by applying a single kernel.

[33] In summary, the increase in effective climate sensitivity observed in the MPI-ESM-LR is likely due to a combination of subtle changes in the feedback mechanisms: Both temperature and cloud feedbacks consistently contribute to the increase in climate sensitivity, regardless of which kernel is used. Depending on whether we use a combination of the CTRL-state kernel and the $4xCO_2$-state kernel, or a constant

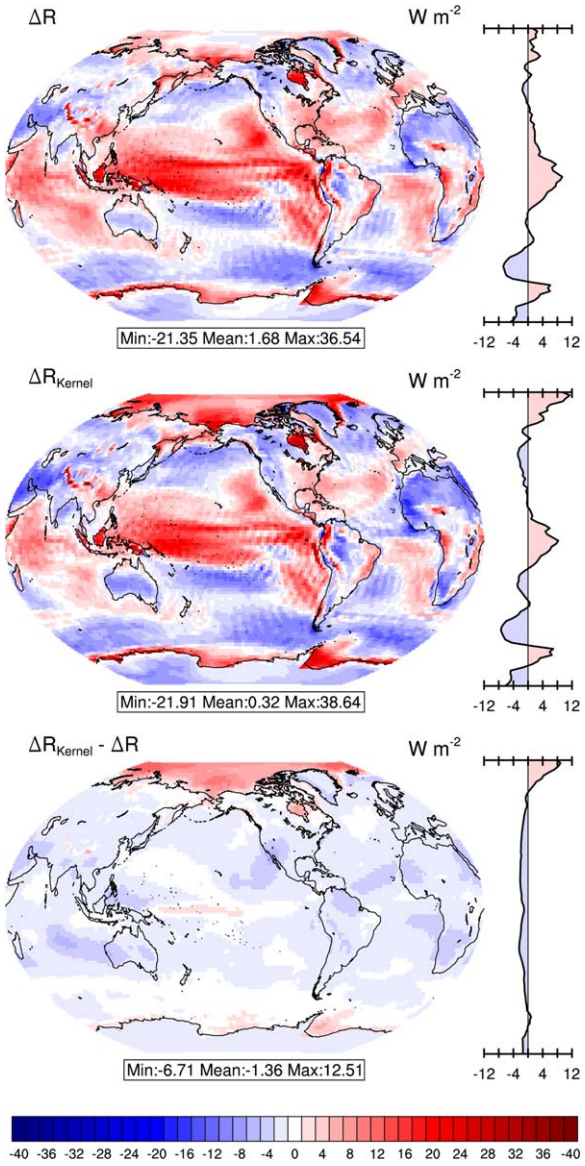

Figure 13. Comparison of (middle) net TOA imbalance ΔR estimated using the CTRL-state kernel to the (top) result given by the model. (bottom) The difference between these two estimates is shown. All results show the mean radiative imbalance of the last 30 years of the 150 year long simulation in the MPI-ESM-LR coupled model with abruptly quadrupled CO_2. Zonal means are shown next to the maps. Positive values indicate energy input in the climate system.

kernel during the entire simulation, we get different results concerning the water vapor and surface albedo feedbacks. Because the spatial distribution of the total model-derived feedback change (Figure 14, top left) indicates a positive shift in feedback in the Arctic region we infer that the surface albedo feedback does likely contribute positively, albeit to a lesser extent than indicated by the analysis using the CTRL-state kernel alone.

4. Conclusions

[34] We have used a combination of the linearized radiative Kernel technique and the Gregory analysis to quantify feedbacks and fast adjustments in the MPI-ESM-LR coupled climate model in a run with abruptly quadrupled CO_2. This was done by assuming a piecewise linear relationship between TOA radiation imbalance and global mean surface temperature before and after two decades into the simulation, and applying radiative kernels to estimate the contributions to forcing and feedback from individual mechanisms. We find positive adjustments from temperature and clouds, both contributing considerably to and almost double the total adjusted CO_2 forcing. The temperature adjustment originates mainly in the well-known stratospheric adjustment, combined with a weak nonnegligible negative tropospheric adjustment from fast warming over land relative to the oceans. Changing water vapor and surface albedo contribute little to the forcing, and can both be considered purely surface temperature-dependent feedback mechanisms in this model. These findings are in good agreement with *Colman and McAvaney* [2011].

[35] The MPI-ESM-LR model with abruptly quadrupled CO_2 exhibits a marked weakening of the total feedback factor from -1.44 to -0.90 W m^{-2} K^{-1} corresponding to a 60% increase in the piecewise linear effective climate sensitivity after about two decades. We explore the possible causes of this nonlinear behavior, not uncommon to coupled climate models. By applying half the forcing ($2xCO_2$) to the coupled model we find slopes before and after 20 years that are statistically indistinguishable from those with $4xCO_2$, suggesting that decadal adjustments associated with deep ocean heat uptake is key to the problem [*Winton et al.,* 2010]. However, when the model is instead coupled to a mixed-layer ocean the models equilibrium climate sensitivity increases by 45% in the second CO_2 doubling relative to the first doubling. As these experiments do not include a representation of the deep ocean, the results suggest instead that processes underlying the feedback mechanisms are state dependent, which is further supported by Cess experiments with prescribed uniform SST warming.

[36] We broke down the total feedback factor change into its individual contributions and show that the increasing effective climate sensitivity in MPI-ESM-LR is likely due to subtle changes in all of the feedback mechanisms: The negative temperature feedback factor consistently weakens, while the positive cloud feedback factor strengthens, thereby both contributing to the increase of effective climate sensitivity, regardless of the choice of radiative kernels. Surface albedo feedback derived from a single kernel suggest a strong increase in the corresponding feedback factor, while when accounting for the increased high-latitude cloudiness in a warmer climate this effect is much less pronounced. Nevertheless, the spatial structure of total feedback does lend support to a weak increase in the surface albedo feedback. Further, the spatial structure reveals that the Southern Ocean in the coupled model counteracts the total

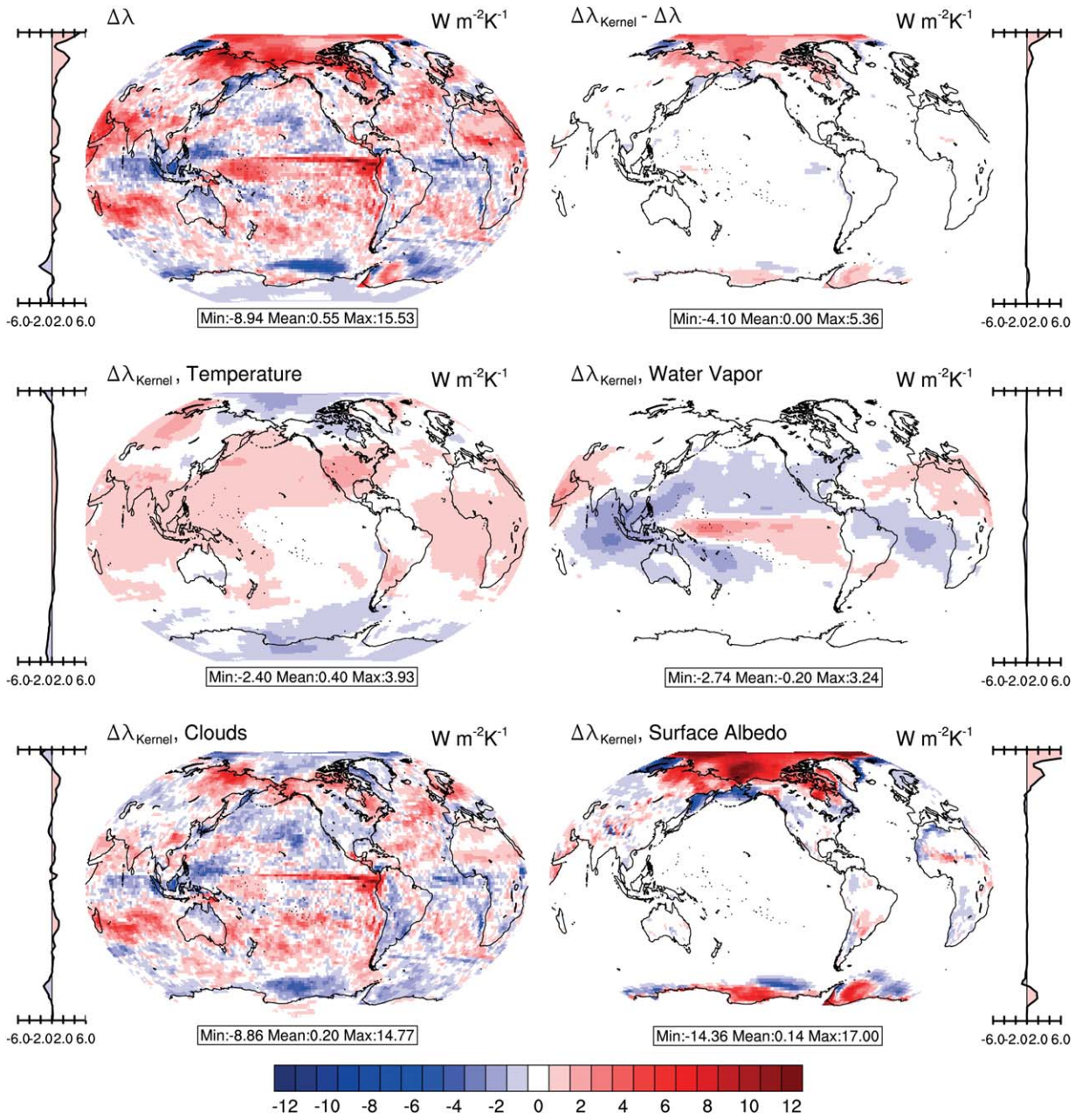

Figure 14. Change in kernel-derived MPI-ESM-LR abrupt 4xCO2 feedback factors $\Delta\lambda$ (the last 130 years minus the first 20 years of the simulation). Red indicates a positive change in the latter part of the simulation. (top right) The sum of the kernel-derived difference in total feedback factor (not shown) minus (top left) the change in total feedback factor derived from the model's TOA radiation imbalance. (middle and bottom) The changes in kernel-derived feedback factors for each individual component. Zonal means are shown next to the maps. Here the CTRL-state radiative kernels are used.

feedback change instead of driving it, as was otherwise suggested by *Senior and Mitchell* [2000].

[37] Limitations of the linear radiative kernel method prohibits a more quantitative analysis of the shifts in the individual feedback factors at this stage, and consequently whether the water vapor feedback increases or decreases in the warmer part of the simulation remains subject to interpretational issues. In the future, it would be interesting to explore warm climates with the PRP method, which does not rely on a linearization and thus may provide more accurate estimates of the water vapor feedback. Indeed, understanding the physical mechanisms underlying the nonlinearities of the feedback mechanisms contributing to the increase in effective climate sensitivity is important as projections of future CO_2 concentrations are not limited to the linear regime of this model—tentatively a doubling of the preindustrial level.

[38] **Acknowledgments.** The authors are grateful for comments and help from Bjorn Stevens, Lorenzo Tomassini, Robert Pincus, Aiko Voigt, Sebastian Rast, Karen Shell, and an anonymous reviewer. This work was supported by the Max Planck Gesellschaft (MPG), and computational resources were made available by Deutsches Klimarechenzentrum (DKRZ) through support from Bundesministerium für Bildung und Forschung (BMBF).

References

Abbot, D. S., C. C. Walker, and E. Tziperman (2009), Can a convective cloud feedback help to eliminate winter sea ice at high CO_2 concentrations?, *J. Clim.*, *22*, 5719–5731, doi:10.1175/2009JCLI2854.1.

Andrews, T., J. M. Gregory, M. J. Webb, and K. E. Taylor (2012), Forcing, feedbacks and climate sensitivity in CMIP5 coupled atmosphere-ocean climate models, *Geophys. Res. Lett.*, *39*, L09712, doi:10.1029/2012GL051607.

Arrhenius, S. (1896), On the influence of carbonic acid in the air upon the temperature of the ground, *Philos. Mag. J. Sci.*, *5*, 237–276.

Cess, R. D., et al. (1990), Intercomparison and interpretation of climate feedback processes in 19 atmospheric general circulation models, *J. Geophys. Res.*, *95*, 16,601–16,615, doi:10.1029/JD095iD10p16601.

Colman, R. A. (2003), A comparison of climate feedbacks in general circulation models, *Clim. Dyn.*, *20*, 865–873, doi:10.1007/s00382-003-0310-z.

Colman, R. A., and B. J. McAvaney (1997), A study of general circulation model climate feedbacks determined from perturbed sea surface temperature experiments, *J. Geophys. Res.*, *102*(D16), 19,383–19,402, doi:10.1029/97JD00206.

Colman, R. A., and B. J. McAvaney (2009), Climate feedbacks under a very broad range of forcing, *Geophys. Res. Lett.*, *36*, L01702, doi:10.1029/2008GL036268.

Colman, R. A., and B. J. McAvaney (2011), On tropospheric adjustment to forcing and climate feedbacks, *Clim. Dyn.*, *36*, 1649–1658, doi:10.1007/s00382-011-1067-4.

Dommenget, D. (2012), Analysis of the model climate sensitivity spread forced by mean sea surface temperature biases, *J. Clim.*, *25*, 7147–7162, doi:10.1175/JCLI-D-11–00600.1.

Dufresne, J.-L., and S. Bony (2008), An assessment of the primary sources of spread of global warming estimates from coupled atmosphere-ocean models, *J. Clim.*, *21*, 5135–5144, doi:10.1175/2008JCLI2239.1.

Eisenman, I., T. Schneider, D. S. Battisti, and M. Bitz (2011), Consistent changes in the sea ice seasonal cycle in response to global warming, *J. Clim.*, *24*, 5325–5335, doi:10.1175/2011JCLI4051.1.

Forster, P., et al. (2007), Changes in atmospheric constituents and in radiative forcing, in *Climate Change 2007: The Physical Science Basis*, Contribution of Working Group I to the Fourth Assessment Report of the Intergovernmental Panel on Climate Change [Solomon, S., D. Qin, M. Manning, Z. Chen, M. Marquis, K.B. Averyt, M. Tignor and H.L. Miller (eds.)], pp. 129–234, Cambridge Univ. Press, Cambridge, U. K. and New York, NY, USA.

Gettelman, A., J. E. Kay, and K. M. Shell (2012), The evolution of climate sensitivity and climate feedbacks in the community atmospheric model, *J. Clim.*, *25*, 1453–1469, doi:10.1175/JCLI-D-11–00197.1.

Giorgetta, M., et al. (2013), Climate change from 1850 to 2100 in MPI-ESM simulations for the coupled model intercomparison project phase 5, *J. Adv. Model. Earth Syst.*, doi:10.1002/jame.20038, in press.

Gregory, J., and M. Webb (2008), Tropospheric adjustment induces a cloud component in CO_2 forcing, *J. Clim.*, *21*, 58–71, doi:10.1175/2007JCLI1834.1.

Gregory, J. M., W. J. Ingram, M. A. Palmer, G. S. Jones, P. A. Stott, R. B. Thorpe, J. A. Lowe, T. C. Johns, and K. D. Williams (2004), A new method for diagnosing radiative forcing and climate sensitivity, *Geophys. Res. Lett.*, *31*, L03205, doi:10.1029/2003GL018747.

Hansen, J., M. Sato, and R. Ruedy (1997), Radiative forcing and climate response, *J. Geophys. Res.*, *102*, 6831–6864, doi:10.1029/96JD03436.

Hansen, J., et al. (2005), Efficacy of climate forcings, *J. Geophys. Res.*, *110*, D18104, doi:10.1029/2005JD005776.

Hartmann, D. L., and K. Larson (2002), An important constraint on tropical cloud—Climate feedback, *Geophys. Res. Lett.*, *29*(20), 1951, doi:10.1029/2002GL015835.

Held, I. M., and B. J. Soden (2000), Water vapor feedback and global warming, *Ann. Rev. Energy Environ.*, *25*, 441–475, doi:10.1146/annurev.energy.25.1.441.

Jonko, A., K. Shell, B. Sanderson, and G. Danabasoglu (2012), Climate feedbacks in CCSM3 under changing CO_2 forcing. Part I: Adapting the linear radiative kernel technique to feedback calculations for a broad range of forcings, *J. Clim.*, *25*, 5260–5272, doi:10.1175/JCLI-D-11–00524.1.

Jonko, A., K. Shell, B. Sanderson, and G. Danabasoglu (2013), Climate feedbacks in CCSM3 under changing CO_2 forcing. Part II: Variation of climate feedbacks and sensitivity with forcing, *J. Clim.*, *26*, 2784–2795, doi:10.1175/JCLI-D-12–00479.1.

Klocke, D., J. Quaas, and B. Stevens (2013), Assessment of different metrics for physical climate feedbacks, *Clim. Dyn.*, doi:10.1007/s00382-013-1757-1, in press.

Mauritsen, T., R. G. Graversen, D. Klocke, P. L. Langen, B. Stevens, and L. Tomassini (2013), Climate feedback efficiency and synergy, *Clim. Dyn.*, doi:10.1007/s00382-013-1808-7, in press.

Moss, R. H., et al. (2010), The next generation of scenarios for climate change research and assessment, *Nature*, *463*, 747–756, doi:10.1038/nature08823.

Pierrehumbert, R. T. (2011), Infrared radiation and planetary temperature, *Phys. Today*, *64*, 1–33.

Senior, C. A., and J. F. B. Mitchell (2000), The time-dependency of climate sensitivity, *Geophys. Res. Lett.*, *27*, 2685–2688, doi:10.1029/2000GL011373.

Shell, K. M., J. T. Kiehl, and C. A. Shields (2008), Using the radiative kernel technique to calculate climate feedbacks in NCAR'S community atmospheric model, *J. Clim.*, *21*, 2269–2282, doi:10.1175/2007JCLI2044.1.

Soden, B. J., and I. M. Held (2006), An assessment of climate feedbacks in coupled ocean-atmosphere models, *J. Clim.*, *19*, 3354–3360, doi:10.1175/JCLI3799.1.

Soden, B. J., A. J. Broccoli, and R. S. Hemler (2004), On the use of cloud forcing to estimate cloud feedback, *J. Clim.*, *17*, 3661–3665, doi:10.1175/1520-0442(2004)017 <3661:OTUOCF >2.0.CO;2.

Soden, B. J., I. M. Held, R. Colman, K. M. Shell, J. T. Kiehl, and C. A. Shields (2008), Quantifying climate feedbacks using radiative kernels, *J. Clim.*, *21*, 3504–3520, doi:10.1175/2007JCLI2110.1.

Stevens, B. et al. (2013), The atmospheric component of the MPI-M earth system model: ECHAM6, *J. Adv. Model. Earth Syst.*, *5*, 46–172, doi:10.1002/jame.20015.

Stuber, N., R. Sausen, and M. Ponater (2001), Stratosphere adjusted radiative forcing calculations in a comprehensive climate model, *Theor. Appl. Climatol.*, *68*, 125–135.

Taylor, K. E., R. J. Stouffer, and G. A. Meehl (2012), An overview of CMIP5 and the experiment design, *Bull. Am. Meteorol. Soc.*, *93*, 485–498, doi:10.1175/BAMS-D-11–00094.1.

Wetherald, R. T., and S. Manabe (1988), Cloud feedback processes in a general circulation model, *J. Atmos. Sci.*, *45*, 1397–1415, doi:10.1175/1520-0469(1988)045 <1397:CFPIAG >2.0.CO;2.

Williams, K. D., W. J. Ingram, and J. M. Gregory (2008), Time variation of effective climate sensitivity in GCM's, *J. Clim.*, *21*, 5076–5090, doi:10.1175/2008JCLI2371.1.

Winton, M., K. Takahashi, and I. M. Held (2010), Importance of ocean heat uptake efficacy to transient climate change, *J. Clim.*, *23*, 2333–2344, doi:10.1175/2009JCLI3139.1.

Corresponding author: K. Block, Max Planck Institute for Meteorology, Bundesstrasse 53, DE-20146 Hamburg, Germany. (karoline.block@zmaw.de)